Research Article

Arnaud Peigné, Umberto Bortolozzo, Stefania Residori, Stéphanie Molin*, Pascale Nouchi, Daniel Dolfi and Jean-Pierre Huignard

Adaptive holographic interferometer based on optically addressed spatial light modulator for high-sensitivity optical fiber sensing

DOI 10.1515/aot-2016-0065
Received December 2, 2016; accepted January 23, 2017; previously published online February 23, 2017

Abstract: Adaptive holographic interferometry is a promising method for high-sensitivity phase-modulation measurements in the presence of slow perturbations from the environment. This technique is based on the use of a nonlinear recombining medium. We report the realization of an adaptive holographic interferometer relying on an optically addressed liquid crystal spatial light modulator operating at 1.55 μm. The beam-coupling process that occurs in a GaAs-liquid crystal device, allows obtaining a phase-modulation sensitivity of 200 μrad/sqrt (Hz) at 1 kHz. The interferometer behaves as an optical high-pass filter, with a cutoff frequency of approximately 10 Hz, thus, filtering slow-phase disturbances, such as due to temperature variations or low-frequency fluctuations, and keeping the detection linear without the need of heterodyne or active stabilization. Moreover, owing to the basic principle of holography, this technique can be used with complex wave fronts such as the speckled field reflected by a highly scattering surface or the optical field at the output of a multimode optical fiber. We demonstrate both theoretically and experimentally that using a multimode optical fiber as a sensing element, rather than a single-mode fiber, allows improving the interferometer phase sensitivity. Finally, we present a phase-optical time domain reflectometry (OTDR) optical fiber sensor using the adaptive holographic interferometer.

Keywords: holographic interferometrys; liquid-crystal device; nonlinear wave mixing; optical fiber sensing.

***Corresponding author: Stéphanie Molin,** Thales Research and Technology, 1 avenue Augustin Fresnel, Palaiseau cedex 91767, France, e-mail: stephanie.molin@thalesgroup.com
Arnaud Peigné: Thales Underwater Systems SAS, Sophia Antipolis, Provence-Alpes-Côte d'Azu, France
Umberto Bortolozzo and Stefania Residori: INLN, Université de Nice-Sophia Antipolis, CNRS, 06560 Valbonne, France
Pascale Nouchi and Daniel Dolfi: Thales Research and Technology France, Palaiseau, France
Jean-Pierre Huignard: JphOpto, Paris, France

www.degruyter.com/aot

1 Introduction

Adaptive holographic interferometry (AHI) is a method based on the combination of classical interferometry and nonlinear optics. It provides interesting properties for phase demodulation with simplified architectures. Also reported as self-adaptive holography or two-beam coupling [1], it differs from classical interferometry by the fact that the recombining medium is replaced by a Kerr optical medium. Therefore, the intensity pattern due to the interfering waves is converted into refractive index modulation, leading to diffraction of the incident waves. The main advantages of adaptive interferometers are (i) a linear phase demodulation without requiring feedback electronics and (ii) filtering of parasitic low-frequency phase modulations. Different adaptive interferometer architectures have been proposed using photorefractive crystals [2]. More recently, Sun et al. [3] reported the use of multiple quantum wells for an adaptive holographic system, while another recently proposed approach is based on digital holography, consisting in the association of a CMOS camera with a LCOS (liquid crystal on silicon) spatial light modulator [4]. The extension of the AHI techniques from the visible to the infrared, and, especially, at 1.55 μm, has been considered for the application of the method in conjunction with optical fiber technology and also because the radiation at this wavelength is partially eye safe. At this purpose, photorefractive effects in semiconductors [5, 6] and erbium-doped optical fibers [7] have been proposed as possible candidates to realize AHI at 1.55 μm.

Here, we propose a method that is based on the use of an optically addressed spatial light modulator (OASLM)

based on liquid crystals and specifically designed to operate at 1.55 μm. It consists of a photoconductive medium and a nematic liquid crystal (LC) layer enclosed between two electrodes. OASLMs based on liquid crystals, also called LC light valves, were previously realized for operation in the visible [8]. Our OASLM is characterized by having a continuous semiconductor photo-addressable surface that makes it very convenient for adaptive holography because, when carefully designed, it needs low optical incident intensity and electrical power, and it filters unwanted phase modulation below 10–100 Hz. This feature is particularly interesting to adapt to temperature or slow environmental changes. Moreover, due to the large birefringence of the LC material [9], the diffraction process is efficient, which leads to a good sensitivity of the device for phase-modulation detection. In this paper, we first describe the OASLM and its characterization. Then, we present the sensitivity, linearity, and bandwidth of the adaptive interferometer made by using the OASLM as the recombining medium. Finally, we study the features of the system for optical fiber sensing.

2 Near-infrared optically addressed spatial light modulator

2.1 Description

The liquid crystal spatial light modulator that we have designed to operate at 1.55 μm is composed of an undoped semi-insulating (SI) GaAs substrate as the photo conductor and nematics (E48 from Merck) for the LC layer (Figure 1). The refractive index of the photoconductor is $n_p \approx 3.4$, while the birefringence characterizing the LC layer is $\Delta n = n_e - n_o \approx 0.2$, with $n_e \approx 1.7$ and $n_o \approx 1.5$ the extraordinary and, respectively, the ordinary index. The undoped SI-GaAs has an absorption coefficient ~ 0.1 cm^{-1} at 1.55 μm [10]. It is cut in the form of a thin slab, 400 μm thickness, and 20×25 mm^2 transverse size. The other cell wall is a glass plate. The LC layer has a thickness of 9 μm and have been planar aligned by rubbed 4% wt. PVA deposed on the confining walls. ITO electrodes are deposed on the outer surface of the photoconductor and inner surface of the glass window in order to apply an external bias voltage V_0 across the device. A similar OASLM has previously been shown to present a very sensitive intensity-dependent refractive index change at 1.06 μm [11], while two-wave mixing at the same optical wavelength has recently been reported in a LC light valve with semiconductor substrate [12].

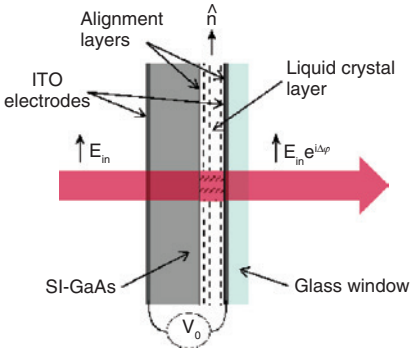

Figure 1: Schematic representation of the optically addressed liquid crystal spatial light modulator (OASLM). It is composed of two ITO electrodes enclosing a semi-insulating (SI) GaAs substrate and a planar-aligned nematic liquid crystal layer. When an optical beam linearly polarized along the nematic director $\hat{n}$ is sent trough the device, it acquires at the output a phase shift $\Delta\varphi$ that depends both on its intensity and on the bias voltage V_0 applied across the OASLM.

2.2 Electrical response

The SI-GaAs substrate provides a photoconductive effect when shone with light at 1.55 μm, therefore allowing to locally increase, in the illuminated regions, the effective voltage V_{LC} dropping across the LC layer. The equivalent simplified electrical circuit of the OASLM is represented in Figure 2A, where R_P, C_P and R_L, C_L represent the resistance

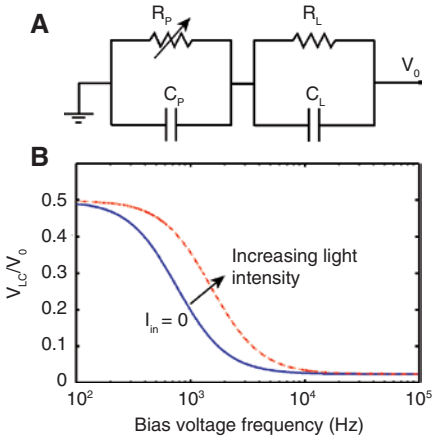

Figure 2: (A) Equivalent electrical circuit of the OASLM: R_p, C_p and R_L, C_L represent the resistance and capacitance of the SI-GaAs substrate and LC layer, respectively; R_p decreases when the 1.55-μm light intensity on the semiconductor substrate is increased. (B) Voltage transfer function versus the bias voltage frequency; the solid (blue) line is calculated for the largest R_p, corresponding to the dark resistivity of the SI-GaAs; the dashed (red) line is calculated for the smallest R_p, corresponding to 10 times the smaller resistivity; R_p varies in between these two values when changing the intensity of the 1.55-μm incident light.

and capacitance of the photoconductive SI-GaAs substrate and LC layer, respectively. PVA layer is very thin (hundreds of nm), and its capacitance does not change with optical intensity. Its contribution to the equivalent electric circuit of the structure is included into C_L. When increasing the intensity of the light impinging on the OASLM, R_P decreases from a maximum value, given by the dark resistivity of the SI-GaAs, to a minimum value, according to the photoconductive coefficient of the material. The largest R_P has been evaluated by taking the photoconductor dark resistivity $\rho_{Pdark} \approx 10^6$ Ωm, while for the smallest value, we consider one order of magnitude less resistivity, consistent with the measured electrical response of the OASLM. When changing the incident light intensity, R_P varies in between these two values. R_L has been calculated by taking the resistivity of the LC layer $\rho_L \approx 10^8$ Ωm. For evaluating C_P and C_L, the low-frequency dielectric constants are taken $\varepsilon_L \approx \varepsilon_P \approx 12$, where for ε_L, we consider the average value between $\varepsilon_{//}$ and $\varepsilon_\perp$. The calculated voltage-transfer function V_{LC}/V_0 is plotted in Figure 2B versus the bias voltage frequency and for the largest and smallest value of R_P. The range of maximum contrast of dark-to-light applied voltage occurs at a driving frequency of approximately 1 kHz. At this frequency, the amplitude that optimizes the optical response is $V_0 \approx 10$ Vrms. For low (high) values of the frequency, the two curves in Figure 2B approach the same level because of the low-frequency (high-frequency) cutoff imposed by the impedances of the dielectric layers of the OASLM.

2.3 Optical response

When V_{LC} increases, molecular reorientation in the LC layer provides a refractive index change that depends both on the incident optical intensity and on the bias voltage V_0 applied across the OASLM. In order to measure the intensity-dependent refractive index change at 1.55 μm, the OASLM has been placed in between cross polarizers oriented at 45° with respect to the LC director orientation. A configuration with two optical beams has been used: a 1.55-μm laser beam, diameter 3.5 mm, was sent directly through the OASLM (transmission T = 0.75%) at different intensities, while a 543-nm probe beam, linearly polarized along the LC director orientation $\hat{n}$, was used to read the induced phase shift. The probe beam was sent on the front side of the OASLM and was retroreflected by the interface between the photoconductor and the LC layer. It had a smaller size (diameter of approximately 1 mm) with respect to the writing beam at 1.55 μm, and it was aligned in order to hit the illuminated area in the middle.

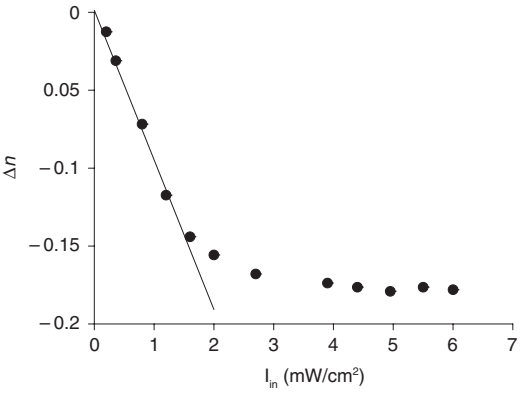

Figure 3: Optical response of the OASLM under 1.55-μm wavelength illumination. Cross: measured data ($V_0 = 8.1$ Vrms at 1 kHz); solid line: linear fit. The light-induced refractive index change is obtained by converting the phase shift measurements on the 1.55-μm transmitted beam and is plotted as a function of the incident optical intensity I_{in}.

Figure 3 shows the intensity-to-index conversion provided by the OASLM $\Delta n = n(I_P) - n_o$. Up to 2 mW/cm², the OASLM responds like a Kerr-like nonlinear medium [13], with a refractive index change proportional to the impinging light intensity. The total refractive index can be expressed in the form $n = n_e + n_2 I_P$, where n_e is the extraordinary index of the LC, n_2 is the nonlinear coefficient characterizing the change produced by the orientational Kerr-like effect in the LC layer, and I_P is the total incident intensity on the photoconductor. By fitting the data, recorded for a bias voltage of 8.1 Vrms at 1 kHz, we obtain $n_e = 1.69$ and $n_2 = -0.2$ cm²/mW. Therefore, for incident intensities in between 0 and 1.5 mW/cm², the OASLM provides a linear conversion of intensity-to-phase modulations, which enables to inscribe intensity fringe patterns inside the LC material.

3 Adaptive holographic interferometer

3.1 Description and principle

The adaptive interferometer is based on two-beam coupling inside the OASLM. As schematically represented in Figure 4A, it consists in a Mach-Zehnder configuration in which the OASLM is the recombining medium. A linearly polarized narrow line-width CW fiber laser at 1.55 μm is divided into two optical paths, forming, respectively, the reference and signal waves of the interferometer.

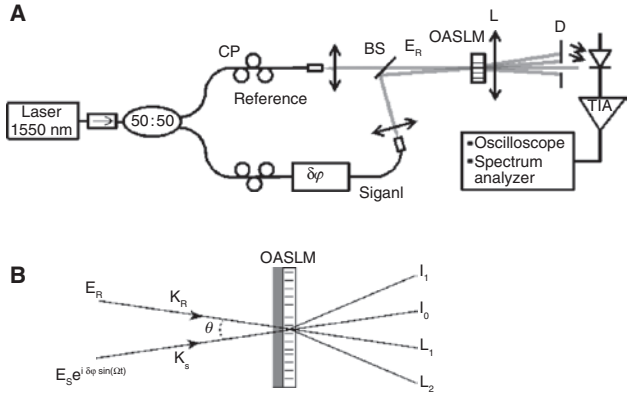

Figure 4: (A) Setup of the adaptive interferometer in a Mach-Zehnder configuration: a 1.55-µm laser source is split into two paths, reference and signal, and, then recombined on the OASLM. In the signal path, it is inserted in a calibrated phase modulator. PC, polarization controller; BS, beam splitter; L, far field lens (focal length 400 mm); D, diaphragm; TIA, trans-impedance amplifier. (B) Schematic representation of the two-beam coupling process occurring in the OASLM.

Collimation free-space optical elements are used to recombine the waves at the entrance of the OASLM, where they have a diameter of 3.5 mm. In one path, identified as the signal arm, it is inserted a calibrated phase modulator that allows introducing a phase modulation $\delta\varphi$. The two interfering waves, of amplitude E_R and, respectively, E_S for the reference and signal, induce a phase grating inside the OASLM through the intensity-to-index conversion occurring in the LC layer and, then, diffract onto the grating.

Diffraction occurs in the Raman-Nath regime, which provides beam coupling and several output orders. Figure 4B shows a schematic representation of the two-beam coupling process occurring in the OASLM. The two waves are phase matched in each diffraction direction and, by measuring with a photodiode the intensity on one of the diffracted orders, linear phase demodulation can be directly achieved. Moreover, due to the response time of the LC, the refractive index grating adapts to slow-phase modulations, thus, the diffracted orders intensities change only for phase modulation above the LC cutoff frequency, and slow perturbations are filtered, keeping the detection linear without the need of heterodyne or active stabilization of the interferometer. The model describing the two-beam coupling process can be derived by considering the total incident intensity on the photoconductor [13]

$$I_P = |E_R e^{i\mathbf{k}_R\cdot\mathbf{r}} + E_S e^{i\,\delta\varphi\,\sin(\Omega t)} e^{i\mathbf{k}_S\cdot\mathbf{r}}|^2, \tag{1}$$

where E_R, E_S are the amplitude of the reference, respectively, signal beam, k_R, k_S their respective propagation wave-vectors, and $\delta\varphi$ is the amplitude of the phase modulation at the frequency Ω. Consequently, the refractive index change $n_2 I_P$ yields a phase grating from which the two beams self-diffract. It can be shown that, if the phase modulation amplitude $\delta\varphi$ is small, then, the mth diffraction order writes [14]

$$I_m = TI_R\left[\eta_m K^2 + \eta_{m+1} + 2K\sqrt{\eta_m\eta_{m+1}}\;\delta\varphi\,\sin(\Omega t)\right], \tag{2}$$

where T is the transmission of the OASLM, $I_R = |E_R|^2$ is the optical intensity of the reference wave, $I_S = |E_S|^2$ is the optical intensity of the signal wave, $K^2 = I_S/I_R$ is the ratio between the input reference and signal intensities, and η_m is the diffraction efficiency of each order m, which can be written as

$$\eta_m = J_m^2(\rho), \tag{3}$$

where $\rho = 2k_0 dn_2 |E_R E_S|$ is the amplitude of the phase excursion in the LC layer, and J_m is the Bessel function of the first kind, order m. Figure 5A shows an example of the observed diffracted orders at the output of the OASLM. In order to detect the phase modulation, the photodiode is placed on the −1 order (indicated by the white arrow), which coincides with the direction of the reference beam. The corresponding measured power spectrum is displayed in Figure 5B, clearly showing the detection of a phase modulation at 1.5 kHz.

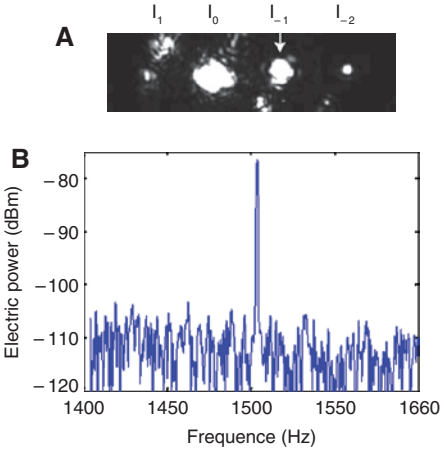

Figure 5: (A) Far-field observation of the diffracted orders in the Raman-Nath regime. The photodiode is placed on the −1 order (indicated by the white arrow), which coincides with the direction of the reference beam. (B) Example of measured power spectrum showing the detection of a phase modulation at 1.5 kHz.

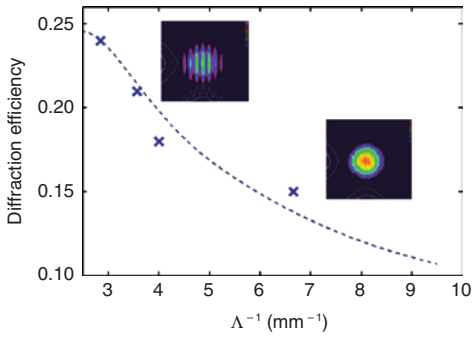

Figure 6: Diffraction efficiency of the self-induced grating as a function of the fringe spatial frequency Λ^{-1}. In the insets are shown the fringe intensity patterns corresponding to $\Lambda = 150$ µm and $\Lambda = 350$ µm. The dashed line is a guide for the eyes.

3.2 Spatial resolution

The minimum fringe spacing Λ for which an efficient phase grating is inscribed in the LC layer is limited by the spatial resolution of the OASLM, which has been evaluated from the diffraction efficiency of the self-induced grating at different angles between the two interfering waves. The diffraction efficiency is plotted in Figure 6 as a function of the fringe spatial frequency Λ^{-1}. The input intensity of the two interfering beams are kept equal $K = 1$, with $I_S = I_R = 0.52\ \mathrm{mW/cm^2}$. The cutoff determines the spatial resolution and can be located at approximately 5 $\mathrm{mm^{-1}}$, corresponding to a fringe spacing of 200 µm. In the following experiments, we set the fringe spacing at 250 µm, which is a good compromise between an efficient beam coupling and an easy separation of diffraction orders at the output of the OASLM. Correspondingly, the angle between the reference and signal beam is 6 mrad.

In order to measure the sensitivity to phase modulation, dynamic range and frequency bandwidth of the interferometer, a calibrated phase modulation $\delta\varphi$ is imposed on the signal beam. In Figure 7A, the optical power measured at the −1 output order is plotted for different phase modulation amplitudes and at a frequency $\Omega/2\pi = 1.5$ kHz. The linearity of the adaptive holographic detection can be clearly appreciated. For a given phase modulation amplitude, and by imposing a signal-to-noise ratio (SNR) equal to unity, it is possible to estimate the sensitivity of the interferometer at 200 µrad/sqrt (Hz). Note that the theoretical shot noise can be evaluated of the order of 20 nrad/sqrt (Hz).

We have also verified that for frequencies above 1 kHz, the sensitivity is limited by the optical source intensity noise. Finally, the frequency bandwidth of the adaptive interferometer has been determined by

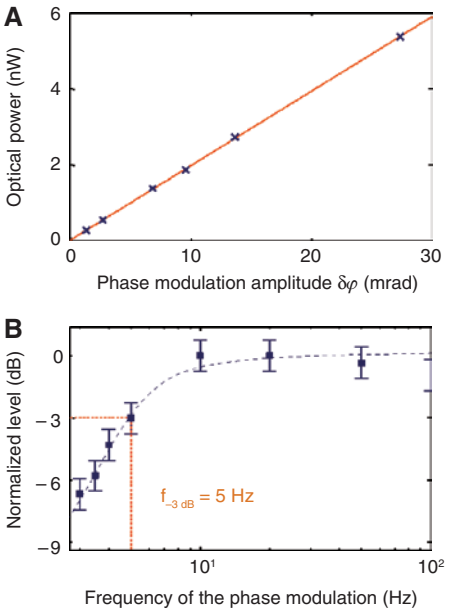

Figure 7: (A) Adaptive holographic detection versus the phase modulation amplitude $\delta\varphi$. The solid line is a linear fit of the data. (B) Frequency bandwidth of the adaptive holographic detection showing the low-frequency cutoff. The dashed line is a guide for the eyes.

measuring the amplitude of the photodiode electrical signal at the phase modulation frequency for different frequencies and at a fixed phase modulation amplitude, $\delta\varphi = 21.6$ mrad.

The results are plotted in Figure 7B. The adaptive interferometer behaves as an optical high-pass filter, with a low-frequency cutoff filtering slow fluctuations. The −3-dB bandwidth can be estimated around 5 Hz. This frequency range can be slightly tuned from tens to hundreds of Hz by acting on the operating parameters of the OASLM (bias voltage, temperature). Consequently, the LC device is particularly adapted to compensate for slow mechanical, temperature, or environmental noise. On the other hand, LC modulators operating in the short and mid infrared have been recently realized by using polymer network liquid crystals and providing response times in the millisecond range [15], thus, opening the possibility of tuning the filter at higher frequencies.

4 Sensitivity enhancement using a multimode optical fiber

Adaptive holography allows the use of complex wave fronts. In particular, it provides a method to measure a phase modulation on a multimode optical fiber (MMF).

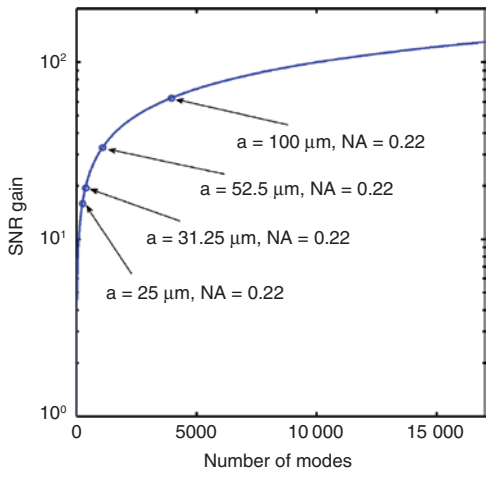

Figure 8: Theoretical SNR gain as a function of the number of propagating modes in the multimode optical fiber. The examples are COTS optical fibers (a, fiber core radius).

If the propagating modes are well injected and if the relative phases of each mode are uncorrelated, the combination of AHI with a multimode fiber can lead to a phase sensitivity enhancement which scales with $\sqrt{N}$, N being the number of modes. We present in Figure 8 the calculated gain on the SNR (at the frequency of the phase modulation applied to the fiber) as a function of the number of modes. We indicate the corresponding commercially available optical fibers in Figure 9. Up to 26 dB of SNR enhancement is expected when using a highly MMF instead of a single-mode fiber. Strain resolution should reach about 0.02 pstrain using a highly MMF instead of a single-mode fiber.

To validate this principle, we built an adaptive holographic interferometer in which a MMF is used in the signal arm (Figure 9). All other fibered parts are single mode. The fiber we used has a core diameter of 105 µm and a numerical aperture of 0.22.

A phase modulation is applied on the fiber, and the diffracted light in the direction of the reference is measured with a photodiode. We show, as an example, the demodulation of a signal at 5 kHz in Figure 10.

We have qualitatively studied the impact of the number of speckle patterns on the SNR. To do so, a diaphragm has been placed in the Fourier plane of the output multimode fiber in order to vary the number of signal beam speckle patterns on the OASLM. For a constant average signal intensity on the OASLM, SNR is measured as a function of diaphragm diameter (Figure 11), evidencing up to 10 dB of SNR gain between the 2.8-mm diameter diaphragm and 1.3-mm diameter diaphragm.

Curves 1–4 in Figure 11 correspond to four measurements with different (arbitrary) injection conditions into the MMF. These observations confirm the Figure 8 results and evidence that SNR can be improved using a great number of speckle patterns on the OASLM. Note that for experimental reasons, SNR gain is not directly compared with the one obtained with a single-mode fiber.

We also have qualitatively studied the impact of speckle intensity distribution on the SNR. The MMF passes through a mode scrambler. Its precision mechanism gently presses the fiber between specially designed corrugated surfaces to cause micro bending of the fiber. This dramatically increases mode coupling among guided

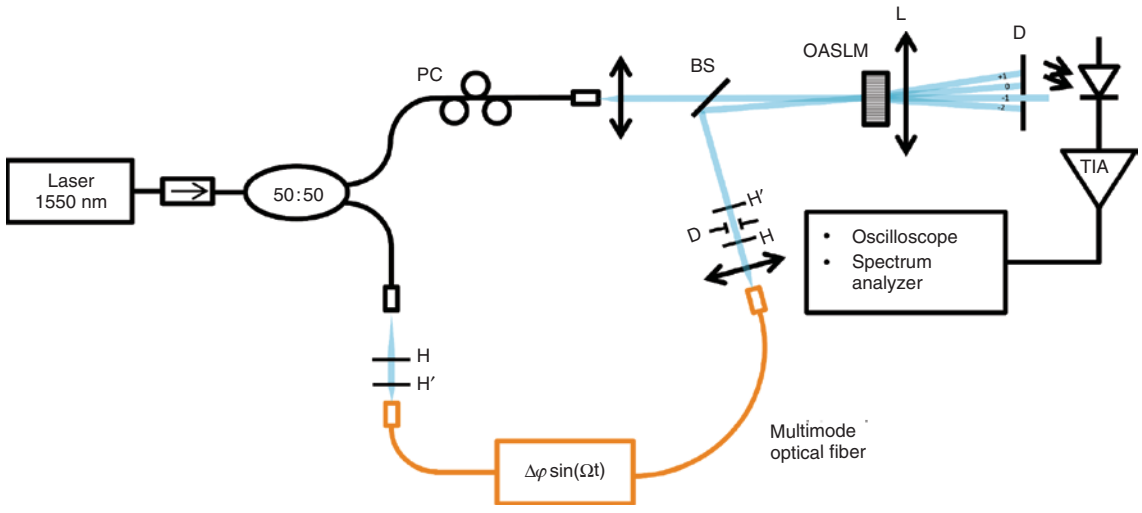

Figure 9: Adaptive holographic interferometer based on a single-mode reference optical path and a multimode signal path. A piezoelectric transducer enables to apply a phase modulation on the signal arm. HH′, free space optics for controlling the beam sizes; D, diaphragm; BS, beam splitter; PC, polarization controller; OASLM, optically addressed spatial light modulator; L, lens for far field.

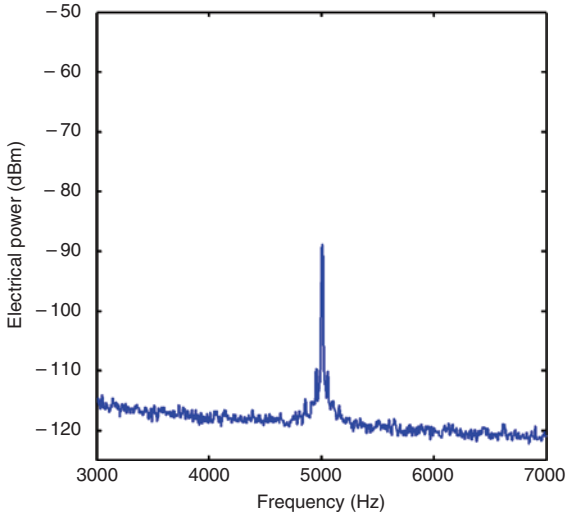

Figure 10: Electrical spectrum of the signal diffracted in the reference direction. The phase modulation is applied to the multimode optical fiber.

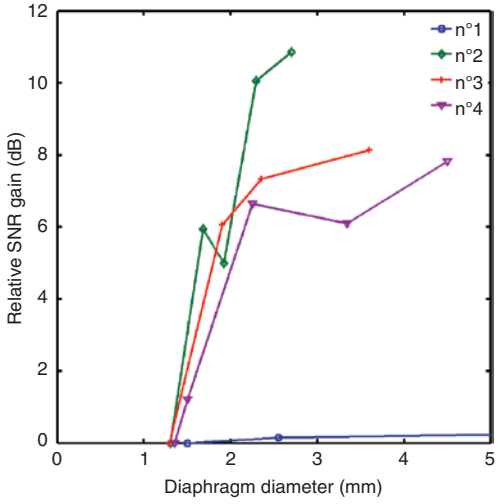

Figure 11: SNR gain (for a phase modulation at 5 kHz on the multimode fiber) as a function of the diaphragm diameter. Curves 1–4 in Figure 11 correspond to four measurements with different (arbitrary) injection conditions into the MMF.

modes. As shown in Figure 12, this device allows stressing the fiber and varying the intensity distribution between the propagating modes.

A phase modulation was applied to the MMF. We measured SNR for different intensity distributions into the MMF. An SNR gain of about 10 dB has been achieved depending on the scrambler-applied stress on the fiber. These observations evidence that SNR varies also depending on speckle pattern intensity distribution. These qualitative measurements using AHI to detect phase modulation applied onto an optical fiber confirm that SNR is enhanced when using a great number of propagating modes.

5 Phase-OTDR-based fiber sensor architecture

Distributed fibers sensors, nowadays, are of great interest for a lot of applications (e.g. oil and gas, avionics, structure health monitoring…). They are based on scattering mechanisms in optical fibers. Among those, fiber sensors based on Rayleigh backscattering offer a good sensitivity and start to be serious candidates for the future generation of numerous distributed sensors. The 'phase-optical time domain reflectometry (OTDR)' method has been proposed by Posey et al. in 2000 [16]. It is based on Rayleigh backscattering in an optical fiber and coherent detection through an interferometer: measurement is made of the phase between the Rayleigh scattered light from two sections of the fiber. The fiber length between these two sections is the 'sensing' length. Recently, the sensitivity of tens of nano strains has been reported with this technique [17]. We propose to investigate this principle by combining it with an adaptive holographic interferometer.

5.1 Theoretical description

The setup, presented in Figure 13, is composed of a laser source, an acousto-optic modulator to obtain optical pulses in the range of hundreds of ns with a repetition rate of hundreds of kHz. The signal is amplified and sent into the sensing fiber through an optical circulator. The single-mode fiber has been used in this experiment, and all fibered components are single mode. The Rayleigh backscattered signal is collected at the circulator port 3, amplified, and sent into the adaptive interferometer. In order to have interference fringes with good visibility on the OASLM, an optical gate is placed before the interferometer input coupler in order to average the light coming from one specific location.

In this way, the interference pattern follows slow changes at this location. The time delay between the input launch pulse and the optical gate opening determines the sensed location of the fiber (see Figure 14). The fiber phase modulation above the cutoff frequency can be measured with a photodiode. Here, we measured the intensity in the direction of the reference wave.

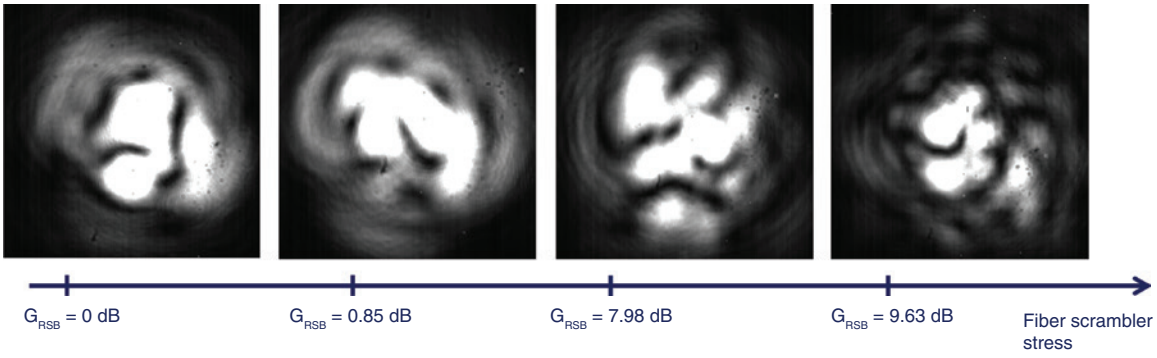

Figure 12: Speckle patterns for four injection conditions and corresponding SNR gain.

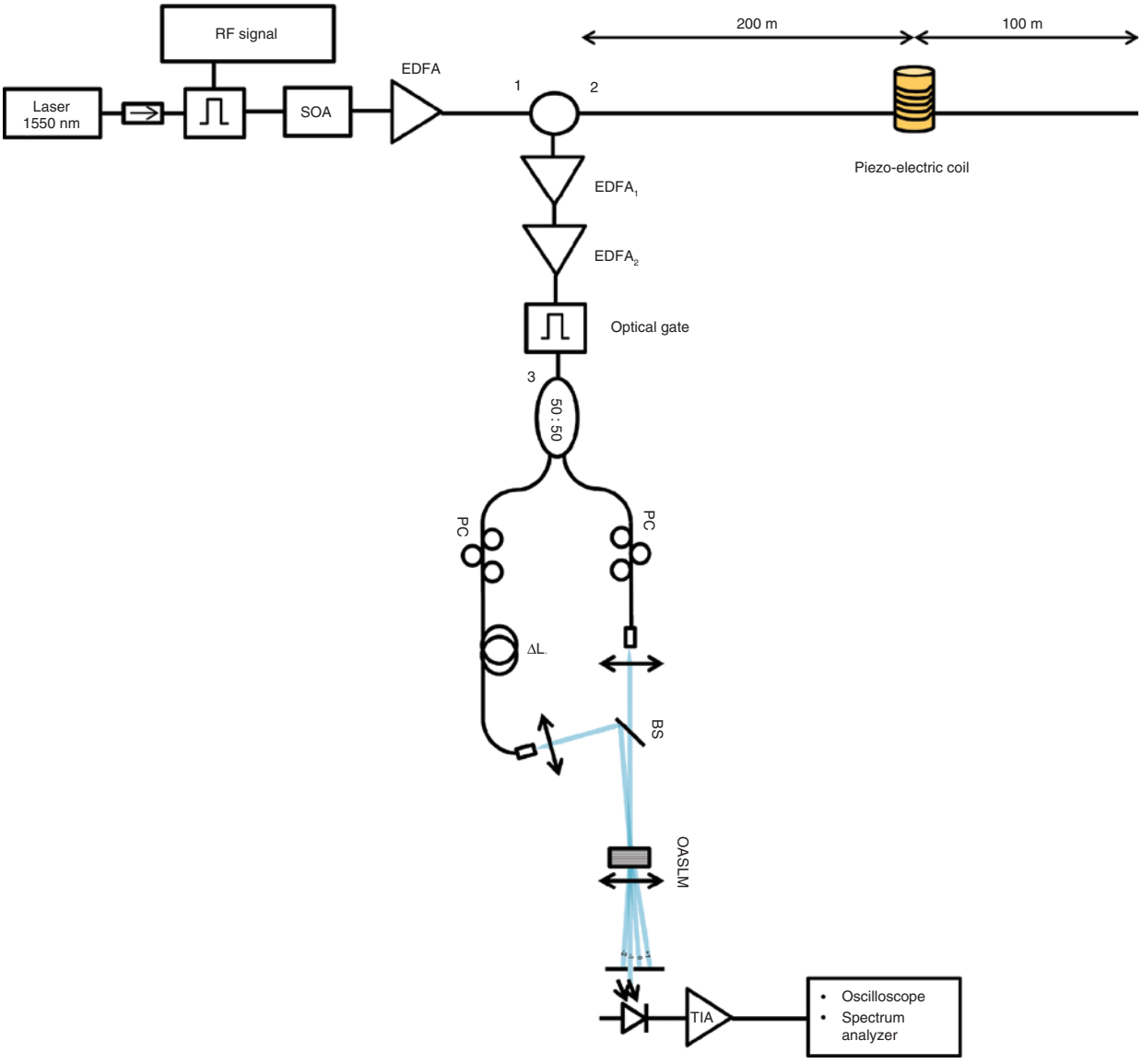

Figure 13: Phase OTDR architecture based on an adaptive holographic interferometer. SOA, semiconductor optical amplifier; EDFA, erbium-doped fiber amplifier.

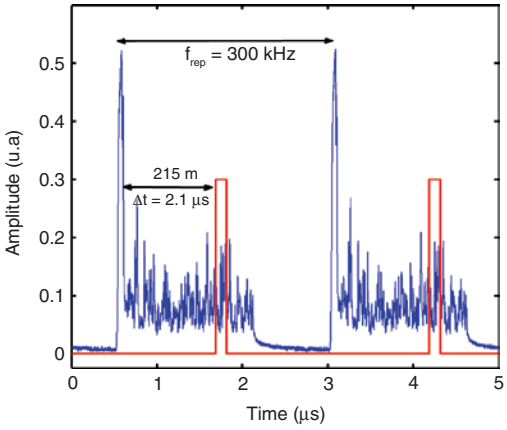

Figure 14: Amplified Rayleigh backscattered trace (blue) and optical gate signal (red). Accumulation of signal recorded during the gate opening allows recording a grating on the OASLM.

5.2 Results

In our experiment, the input pulse duration is 120 ns, and the repetition rate f is set at 300 kHz, i.e. near the limit given by the fiber length through the relation $f < c/2nL$, where n is the effective refractive index, L is the fiber length, and c is the light velocity in vacuum. In our setup, L = 300 m, leading to $f < 340$ kHz. A 1.5-kHz phase modulation (through a piezoelectric cylinder and preliminarily calibrated) is applied at 200 m from the fiber input. The optical path difference in the interferometer sets the spatial resolution of the sensor. For this demonstration, we have $\Delta L = 50$ m giving a spatial resolution of 25 m. The optical power of the laser source is 10 mW. Considering the intensity modulation and the amplifier, the peak power at the input of the fiber is 3 W.

An average intensity near 1.5 mW/cm^2 is necessary to attain the operating point of the OASLM. We need to amplify the backscattered averaged signal with a gain estimated at 30 dB. To do so, a pre-amplifier and an amplifier have been used at the output of the optical circulator. Finally, we have measured the electrical spectrum of the signal delivered by the photodiode for different time delays of the optical gate. We show on Figure 15 the signals obtained successively for two locations. The blue curve is obtained for optical gate open for light coming from 37.5 m to 62.5 m along the sensing fiber. No modulation is observed at 1.5 kHz. The green curve corresponds to light coming from 187.5 m to 212.5 m. A peak is observed at 1.5 kHz corresponding to the sensing fiber phase modulation frequency. Power detected around 1 kHz is due to environmental noise. This noise was fluctuating in the laboratory from one measurement to the other. For both curves, peaks below 500 Hz are spurious. One limitation of this optical fiber sensor architecture comes from the fact that it is not possible to measure the phase modulation at different locations in the fiber simultaneously. However, we can easily retrieve the modulation peak at 1.5 kHz corresponding to the frequency of the piezoelectric transducer. We, therefore, demonstrate the possibility of detecting and localizing a phase modulation using AHI combined with phase-OTDR. Phase sensitivity of 10.56 $\text{mrad}/\sqrt{\text{HZ}}$ has been obtained with this setup. Simultaneous localization protocols could be envisaged in the future by realizing more complex architectures.

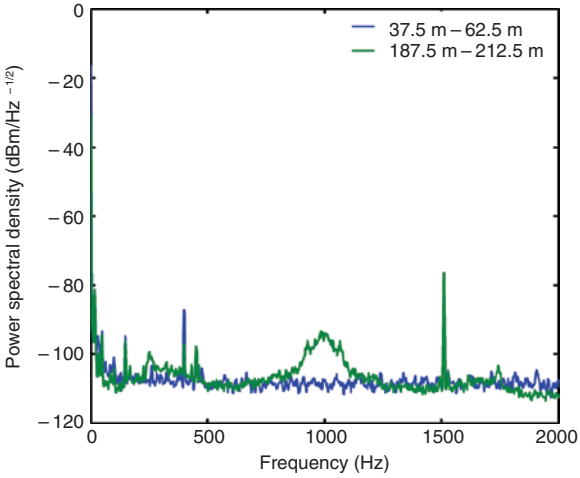

Figure 15: Power spectral density of the diffracted signal at two different locations (corresponding to two different delays of the optical gate). We can see the detected phase modulation between 187.5 and 212.5 m, which corresponds to the phase modulation applied at 200 m (with a spatial resolution of 25 m).

6 Conclusion

In conclusion, we have designed and realized a LC spatial light modulator operating at 1.55 µm, which is particularly suited for acting as the recombining Kerr-like medium in an adaptive interferometer operating in this range of optical wavelengths. We have shown that the interferometer operates as a high-pass optical filter, with a cutoff frequency in the range of 10 Hz, thus, filtering out slow phase fluctuations and keeping the detection linear. The sensitivity to phase modulations has been estimated to be 200 µrad/sqrt (Hz) at 1 kHz and the filtering frequency cutoff at approximately 5 Hz. These properties, namely, the ability of filtering low-frequency noise and the intrinsic linear detection, make this device a simple and good candidate for sensing applications even in disturbed environment. Because of holography principles, the method

is suitable also for working with complex optical fields, such as those diffracted by multimode optical fibers or diffused by highly scattering objects. We demonstrated SNR enhancement by using a multimode fiber to detect a phase modulation, rather than a single-mode one. Finally, we presented a localization experiment based on a phase-OTDR in a single-mode fiber. Future work will be dedicated to combine AHI and phase-OTDR into a multimode fiber in order to evaluate the sensitivity and the potential of the overall architecture. Particular attention will be dedicated to enhance spatial resolution and to phase localization at several locations along the sensing fiber simultaneously.

Acknowledgments: This work has been supported by the French Délégation Générale de l'Armement (DGA) under contracts ANR-11-ASTR-0012, Astrid MEDUSE, and ANR-14-ASMA-0004-01, Astrid Maturation HYDRE.

References

[1] V. L. Vinetskii, N. V. Kukhtarev, S. G. Odulov and M. S. Soskin, Sov. Phys. Usp. 22, 742–756 (1979).
[2] A. A. Kamshilin, R. V. Romashko and Y. N. Kulchin, J. Appl. Phys. 105, 031101 (2009).
[3] H. Sun, D. D Nolte, J. Hyland and E. Harmon, Proc. SPIE 8619, 86190E (2013).
[4] U. Bortolozzo, D. Dolfi, J. P. Huignard, S. Molin, A. Peigné, et al., Opt. Lett. 40, 1302 (2015).
[5] P. Delaye, L.-A. de Montmorillon and G. Roosen, Opt. Commun. 118, 154 (1995).
[6] M. B. Klein, K. V. Shcherbin and V. Danylyuk, in 'OSA Trends in Optics and Photonics (TOPS), Photorefractive Effects, Materials, and Devices', Ed. By P. Delaye, C. Denz, L. Mager and G. Montemezzani (OSA, Washington, DC, 2003), Vol. 87, pp. 483–489.
[7] J. Lòpez Rivera, M. Plata Sànchez, A. Miridonov and S. Stepanov, Opt. Express 21, 4280 (2013).
[8] P. Aubourg, J. P. Huignard, M. Hareng and R. A. Mullen, Appl. Opt. 21, 3706–3712 (1982).
[9] I. C. Khoo, Liquid Crystals: Physical Properties and Nonlinear Optical Phenomena, second edition, (Wiley Interscience, New York, 2007).
[10] P. Delaye, L. A. de Montmorillon, H. J. Bardeleben and G. Roosen, Appl. Phys. Lett. 64, 2640 (1994).
[11] U. Bortolozzo, S. Residori and J. P. Huignard, Appl. Opt 52, 220E73-05 (2013).
[12] K. Shcherbin, I. Gvozdovskyy and D. R. Evans, Communication at the Photorefractive Photonics Meeting, PR15, Villars, Switzerland, June 16–19 (2015).
[13] U. Bortolozzo, S. Residori and J. P. Huignard, Laser Photonics Rev. 4, 483–498 (2010).
[14] U. Bortolozzo, S. Residori and J. P. Huignard, Opt. Lett. 34, 2006 (2009).
[15] J. Sun and S.-T. Wu, J. Polym. Sci., Part B: Polym. Phys. 52, 183–192 (2013).
[16] R. J. Posey, G. A. Johnson and S. T. Vohra, Electron. Lett. 36, 1688–1689 (2000).
[17] A. Masoudi, M. Belal and T. P. Newson, Meas. Sci. Technol. 24, 085204 (2013).